Conformational Changes in Aerolysin during the Transition from the Water-Soluble Protoxin to the Membrane Channel[†]

Véronique Cabiaux,[‡] J. Thomas Buckley,[§] Ruddy Wattiez,[||] Jean-Marie Ruysschaert,[‡] Michael W. Parker,[⊥] and F. Gisou van der Goot*[,@]

Laboratoire de Chimie Physique des Macromolécules aux Interfaces CP 206/2, Université Libre de Bruxelles, Boulevard du Triomphe, 1050 Bruxelles, Belgium, Department of Biochemistry and Microbiology, University of Victoria, Box 3055, Victoria, British Columbia, Canada V8W 3P6, Department of Biological Chemistry, University of Mons-Hainaut, 21, avenue Maistriau, 7000 Mons, Belgium, The Ian Potter Foundation Protein Crystallography Laboratory, St. Vincent's Institute of Medical Research, 41 Victoria Parade, Fitzroy, Victoria 3065, Australia, and Département de Biochimie, Université de Genève, 30 quai E. Ansermet, 1211 Genève, Switzerland

Received May 23, 1997; Revised Manuscript Received September 25, 1997[⊗]

ABSTRACT: Proteolytic activation, oligomerization, and membrane insertion are three steps that precede channel formation by the bacterial toxin aerolysin. Using attenuated total reflection Fourier transform infrared spectroscopy (ATR-FTIR) and hydrogen−deuterium exchange, the structural changes associated with each step were analyzed. Our results show that activation induces a significant change in secondary structure, characterized by a decrease in random structure and an increase in β-sheet content. We show that release of the propeptide is essential for this conformational change to occur and that changes are not restricted to the vicinity of the cleavage site but appear to propagate along the molecule. In contrast, subsequent oligomerization of the mature toxin does not involve any change in overall secondary structure but does involve a modification of the tertiary interactions. Finally, insertion of the heptameric complex into dimyristoylphosphatidylcholine vesicles also occurs without major modification of the secondary structure. Studies on the orientations of the secondary structures of the heptamer in the lipid bilayer have also been performed.

The channel-forming toxin aerolysin undergoes several conformational changes from the time it is released by the bacterium to the moment it forms a pore in the plasma membrane of a target cell (for review, see ref 1). The protein is secreted as an inactive dimer by the Gram-negative bacterium *Aeromonas hydrophila* (*2*) (Figure 1). The protoxin then reaches its target cell by diffusion, binds to specific receptors (*3*−*6*; L. Abrami, M. Fivaz, and F. G. van der Goot, unpublished) and becomes activated by proteolytic removal of a C-terminal peptide (*7*, *8*). In the next step, aerolysin oligomerizes, and this results in the conversion of the water-soluble dimer to the insertion-competent heptamer (*9*). Oligomer insertion produces discrete channels in the membrane which in cells such as the erythrocyte is followed by osmotic lysis.

The structure of proaerolysin has been determined at atomic resolution (*10*) (Figure 1). The protein consists of two lobes, a small globular lobe (Domain 1, amino acids 1−84) and a more elongated lobe rich in long β-strands that run from one end of the protein to the other. In the dimer, the two Domains 1 clasp each other in a crossover fashion. This domain-swapping interaction is thought to maintain the two monomers together (Figure 1, M. W. Parker et al., unpublished results). On the basis of structural analysis and functional studies, the large lobe of the toxin has been divided into three domains (Domains 2−4). Proteolytic activation occurs in Domain 4 (*7*, *8*), and oligomerization has been shown to depend on amino acids in Domain 2 (*10*).

The structure of mature aerolysin has not yet been determined, either in the dimeric or in the oligomeric form. Low-resolution images of the aerolysin channel have however been obtained from electron micrographs of the two-dimensional crystals of the oligomer associated with *Escherichia coli* phosphatidylethanolamine lipids (*11*), and an atomic model of the channel has been proposed (*10*).

Aside from the available crystallographic data, little is known about the structural modifications occurring during the conversion of dimeric proaerolysin to the heptameric aerolysin channel. In this study, we have analyzed the conformational changes that occur upon proteolytic activation, oligomerization, and membrane insertion using attenuated total reflection Fourier transform infrared (ATR-FTIR) spectroscopy. FTIR appears to be the method of choice for analyzing these conformational changes since aerolysin is too large for NMR studies and since attempts to crystallize the aerolysin heptamer have not yet been successful. Moreover, FTIR can be applied in the presence of lipids.

EXPERIMENTAL PROCEDURES

Purification. Wild type and mutant proaerolysins were purified as described previously (*12*). Generation of H132D, G202C/I445C, and M41C mutant toxins was previously

[†]This work has been supported by grants from the Swiss National Science Foundation (F.G.v.d.G.) and from the National Sciences and Engineering Research Council of Canada (J.T.B.). V.C. is a research associate of the National Fund for Scientific Research (Belgium).

* To whom correspondence should be addressed. Telephone and fax: (41) 022 702-6414. E-mail: Gisou.vandergoot@biochem.unige.ch.

[‡] Université Libre de Bruxelles.

[§] University of Victoria.

[||] University of Mons-Hainaut.

[⊥] St. Vincent's Institute of Medical Research.

[@] Université de Genève.

[⊗] Abstract published in *Advance ACS Abstracts,* November 1, 1997.

S0006-2960(97)01216-6 CCC: $14.00

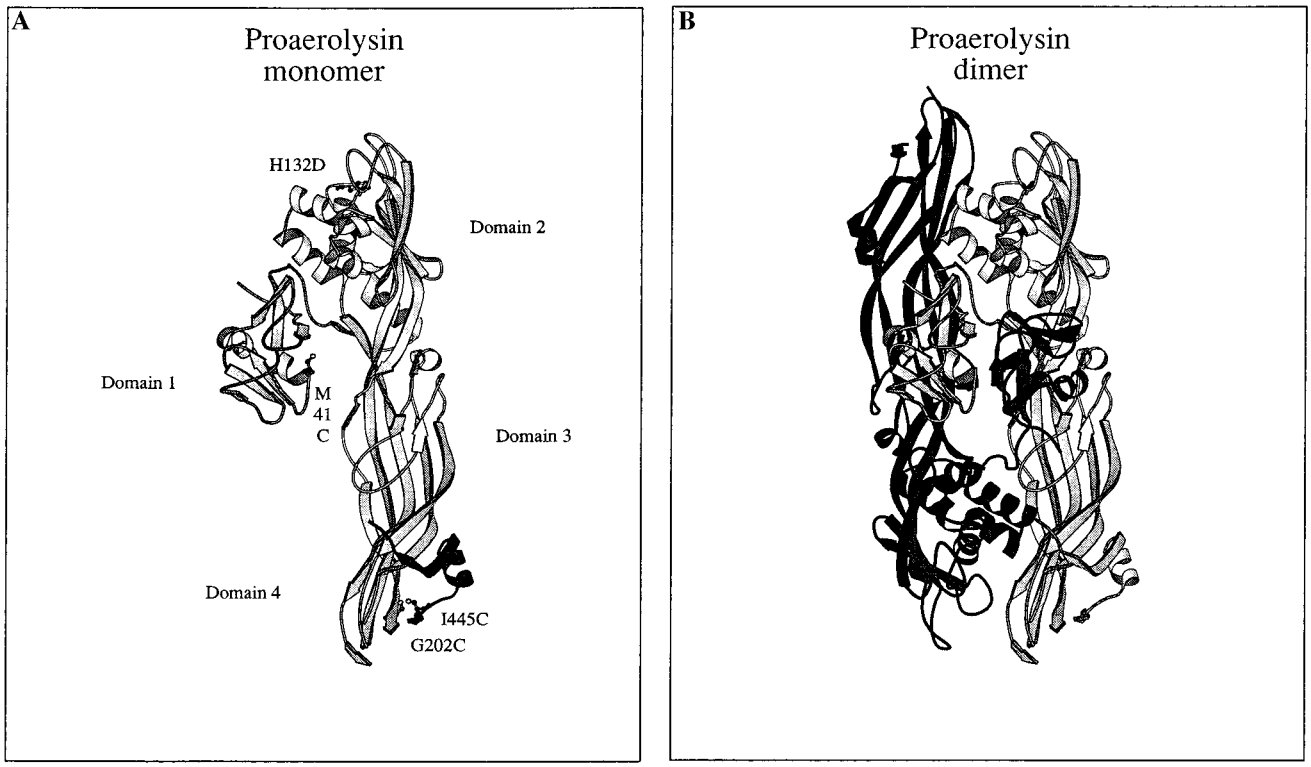

FIGURE 1: Structure of proaerolysin. The ribbon diagrams of proaerolysin are based on the crystal structure (*10*). (A) Proaerolysin monomer. Residues Met-41, His-132, Gly-202, and Ile-445 are positioned. The propeptide has been darkened (bottom right). (B) Proaerolysin dimer. The two monomers are in gray and black. This figure was prepared using the program MOLSCRIPT (*34*).

described (*13*−*15*). Concentrations were determined by measuring the optical density (OD) at 280 nm. A 1 mg/mL solution of proaerolysin has an OD_{280} of 2.5 (*14*).

Preparation of Dimeric and Heptameric Aerolysin. Wild type or mutant proaerolysin (0.4 mg/mL) was activated by treatment with trypsin attached to cross-linked beaded agarose (Sigma, 0.5 unit of insoluble trypsin per milliliter of solution) for 1 h at room temperature in a buffer containing 150 mM NaCl and 20 mM Tris-HCl at pH 8.4. The sample was then centrifuged to remove the trypsin. To remove the C-terminal peptide that is released upon activation (*14*), the sample was passed down a Sephadex G50 column (Pharmacia Biotech Inc.), and the protein was recovered in the void volume. N-Terminal sequencing of the samples using a Beckman LF3400 protein-peptide microsequencer confirmed that 90% of the propeptide had been removed by this gel filtration step. The protein was then dialyzed against 2 mM *N*-(2-hydroxyethyl)piperazine-*N*′-2-ethanesulfonic acid (HEPES[1]) at pH 7.4 for FTIR studies. Complete conversion of proaerolysin to aerolysin and the oligomerization state of the toxin were assessed by SDS−PAGE. To prepare heptameric aerolysin, wild type proaerolysin was activated as described above and dialyzed against a buffer containing 30 mM NaCl and 20 mM HEPES at pH 7.4 for 18 h at room temperature. This procedure resulted in almost full conversion to the heptameric form as determined by SDS−PAGE (Figure 2A, lane 2).

[1] Abbreviations: HEPES, *N*-(2-hydroxyethyl)piperazine-*N*′-2-ethanesulfonic acid; ATR, attenuated total reflection; UV CD, ultraviolet circular dichroism; FTIR, Fourier transform infrared; DMPC, dimyristoylphosphatidylcholine; H132N, mutant in which histidine 132 has been mutated to asparagine; H132D, mutant in which histidine 132 has been mutated to aspartic acid; M41C, mutant in which methionine 41 has been mutated to cysteine; G202C/I445C, double mutant in which both glycine 202 and isoleucine 445 have been changed to cysteine.

Reconstitution Procedure. The reconstitution protocol was very similar to the one used to generate two-dimensional crystals of the aerolysin (*11*) heptamer. All steps were carried out at room temperature. The NaCl concentration of the heptameric aerolysin sample (approximately 0.4 mg of protein/mL), obtained as described above, was raised to 150 mM. Octyl-POE was then added to 1% (v:v, Bachem), and the mixture was incubated for 30 min using a rotary shaker. Dimyristoylphosphatidylcholine (DMPC) suspended in 150 mM NaCl and 20 mM HEPES at pH 7.4 containing 1% octyl-POE (v:v) was then added to obtain a final protein: lipid ratio of 1:7 (w:w). After 30 min, which allowed formation of mixed micelles between protein, lipid, and detergent, 50 mg/mL SM2 Bio-Beads (Bio-Rad) were added to remove the octyl-POE. After 1 h, another sample of 50 mg/mL beads was added and the incubation was allowed to proceed for an additional 1 h. After removal of the beads, the heptamer−DMPC sample was briefly sonicated using a tip sonicator (3 × 5 s). Sucrose was added to reach 41% (w:w), and a discontinuous flotation gradient was prepared with successive layers of 35, 25, and 0% sucrose in 150 mM NaCl and 20 mM HEPES at pH 7.4. After centrifugation at 35 000 rpm for 1 h in a Beckman SW40 rotor (16 °C), the 35−25% interface containing the proteoliposomes was collected. Although the starting heptameric aerolysin fraction was slightly contaminated with a nonoligomerized population (Figure 2A, lane 2), only the heptameric form was recovered after flotation on the sucrose gradient (Figure 2A, lane 3). The proteoliposomes were then washed with 2 mM HEPES at pH 7.4 by three rounds of centrifugation resuspension (20 min at 55 000 rpm using a Beckman TL100.3 rotor).

Attenuated Total Reflection Fourier Transform Infrared Spectroscopy (ATR-FTIR). Attenuated total reflection infrared spectra were obtained using a Perkin-Elmer 1720X

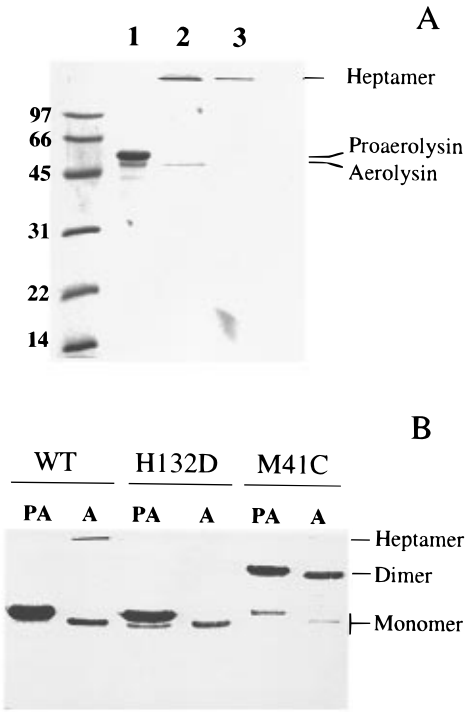

FIGURE 2: Different forms of aerolysin. (A) Reconstitution of the aerolysin heptamer into DMPC vesicles. Analysis by SDS−PAGE (15%) showed that the heptameric aerolysin, obtained by extensive dialysis as described in Experimental Procedures, still contained a slight contamination of nonoligomerized toxin (lane 2). However, only the heptamer was reconstituted in DMPC vesicles and recovered on the sucrose gradient at the 25−35% sucrose interface (lane 3). Note that the aerolysin heptamer (332 kDa) is stable in SDS and therefore runs at a very high molecular mass. In contrast, the proaerolysin and aerolysin dimers are sensitive to SDS and run as monomers. Lane 1, proaerolysin marker containing a small amount of aerolysin. (B) Nonoligomerizing aerolysin mutants. Aerolysin (A) was obtained by treating proaerolysin (PA) with trypsin followed by removal of the propeptide by gel filtration as described in Experimental Procedures. No oligomers could be detected for the two mutants, in agreement with previous data (*13*, *15*, *26*). A sample of wild type aerolysin containing both heptamers and dimers is shown as a control. All samples were prepared in sample buffer containing β-mercaptoethanol except for the M41C samples in which the reducing agent was omitted. The M41C mutant therefore migrates as a dimer. The wild type and H132D dimers are not stable in SDS, and the proteins migrate as monomers.

FTIR spectrophotometer equipped with a liquid nitrogen-cooled mercury cadmium telluride detector at a resolution of 4 cm^{-1}. The spectrophotometer was continuously purged with air passed through a silicagel column to remove water vapor. The internal reflection element was a germanium ATR plate (50 × 20 × 2 mm, Harrick EJ 2121) with an aperture angle of 45°, yielding 25 internal reflections. Thin films were obtained by slowly evaporating 50 μL of the sample under a stream of nitrogen on one side of the ATR plate (*16*, *17*) which was then sealed in a universal sample holder (Perkin-Elmer model 186-0354). For deuteration, the sample compartment was flushed with D_2O-saturated N_2 at room temperature. Exchange of hydrogen with deuterium makes it possible to differentiate α-helical components from random structure, since the absorption of the latter shifts from about 1655 to about 1642 cm^{-1} upon deuteration (*18*). The frequency limits for the different structures were as follows: 1662−1645 cm^{-1} for α-helix, 1689−1682 and 1637−1613 cm^{-1} for β-sheet, 1644.5−1637 cm^{-1} for random structure, and 1682−1662.5 cm^{-1} for β-turns (*19*). Each measurement was the average of 128 scans.

Table 1: Solvent Accessibility Calculations[a]

form	surface of a monomer (Å^2)
precursor dimer (proaerolysin)	19 990
mature dimer (aerolysin)	19 268
heptamer	18 719[b]
	16 057[c]

[a] Solvent accessibility calculations were performed with the program DSSP (*24*). Surface areas are averages of the two accessible surfaces calculated for the two monomers in the dimer. [b] The solvent accessibility was calculated without taking into account the presence of the lipid bilayer. [c] Corresponds to the surface accessibility of the monomer in the heptamer assuming that Domain 4 is entirely embedded into the membrane. The solvent accessibility through the lumen of the channel was not taken into account.

Kinetics of Deuteration. Experiments were carried out as previously described (*20*). At time zero, a D_2O-saturated N_2 flux was applied to the sample, with a flow rate of 75 mL/min, controlled with a Brooks flow meter. The spectra at each kinetic point were the accumulation of 12 scans. The background due to the atmospheric water contribution, as well as the contribution of the lateral side chains, was subtracted from each spectrum (*20*). The amide I and II band areas were measured between 1702 and 1596 cm^{-1} and 1585 and 1502 cm^{-1}, respectively. For each spectrum, the amide II area was divided by the amide I area to take into account changes in the total intensity during the deuteration process. The amide II:amide I ratio, expressed between 0 and 100%, was plotted as a function of deuteration time. The 100% value was defined by the amide II:amide I ratio obtained before deuteration, whereas the 0% value corresponded to a zero absorption in the amide II region. It has been shown on a series of proteins which can be fully unfolded (and therefore fully deuterated in the denatured state) and then refolded to their native state that complete H−D exchange results in 0 ± 5% absorption in the amide II region (*21*, *22*).

Other Methods. SDS−PAGE was performed as described by Laemmli (*23*). Calculation of surface accessibility was performed with the program DSSP (*24*).

RESULTS

Structural Effects of Activation. H132D proaerolysin was used to analyze the structural changes associated with activation and avoid the potentially confounding effects of oligomerization. In contrast to wild type aerolysin, the mature form of H132D is unable to form oligomers spontaneously in solution (Figure 2B) (*13*, *25*, *26*). Mutation of His-132 does not affect the structure of proaerolysin since H132N, which has properties identical with that of H132D, has the same crystallographic structure as the wild type toxin (M. W. Parker et al., unpublished observation). Also, H132D and wild type proaerolysins were found to have the same FTIR spectra (spectra a in Figures 3A and 6A, respectively) as well as the same near- and far-UV CD spectra (not shown). In fact, the inability to oligomerize is due to the fact that protonation of His-132 is required for polymerization (*26*). As expected from the crystal structure, the spectrum of H132D proaerolysin showed that the protein is rich in β-structure (maximum of absorption at 1633 cm^{-1}) but that it also contains a significant amount of α-helical structure

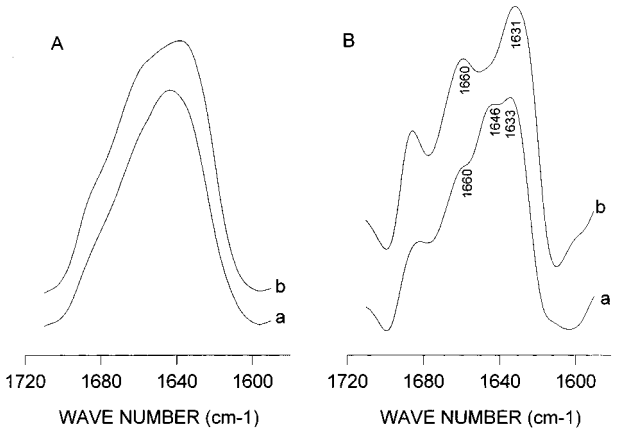

FIGURE 3: Deuterated FTIR spectra of H132D proaerolysin and aerolysin. Aerolysin was obtained by treating proaerolysin with trypsin, and the propeptide was removed by gel filtration as described in Experimental Procedures. The spectra of proaerolysin and mature aerolysin mutants were recorded on thin films and taken after the end of the measurements of the corresponding kinetics of deuteration (Figure 4). For all spectra, a linear baseline was subtracted between 1705 and 1595 cm^{-1}. (A) Original spectra of H132D proaerolysin (a) and aerolysin (b). (B) Deconvoluted spectra of H132D proaerolysin (a) and aerolysin (b) with a resolution factor *K* of 2.2.

(absorption at 1660 cm^{-1}) (Figure 3). Conversion of H132D proaerolysin to aerolysin by trypsin led to a significant change in the FTIR spectrum, evidence that a conformational change occurred (Figure 3). Thus, the proaerolysin spectrum had three main absorption bands, at 1660, 1646, and 1633 cm^{-1} (Figure 3B, spectrum a), characteristic of α-helical, random coil, and β-sheet structure, respectively, whereas the main absorption maxima for aerolysin occurred at 1660 and 1631 cm^{-1} (Figure 3B, spectrum b). Evaluation of the secondary structures of both forms of the protein by Fourier self-deconvolution and curve fitting (*19*) revealed a 10 ± 5% increase in β-sheet content upon activation, with a concomitant decrease in the amount of "random" structure. Similar differences between the spectra of proaerolysin and aerolysin were observed prior to deuteration, indicating that the observed change is not a deuteration artifact (data not shown). The change in secondary structure observed here cannot be accounted for by the mere loss of the C-terminal peptide, since the relative proportions of the different secondary structure elements calculated from the X-ray structure are essentially the same whether the peptide is taken into account (not shown).

Activation of H132D did not lead to a significant change in the exchangeability of peptide hydrogens for deuterium (Figure 4). Both the kinetics and the extent of deuteration were very similar for pro and mature H132D. About 60% of the residues were exchanged after 3 h.

The change in secondary structure observed upon activation of the H132D mutant could be due to hydrolysis of the peptide bond by trypsin or to the release of the C-terminal propeptide (*14*) which follows. To determine which alternative accounts for the change, we analyzed the effect of

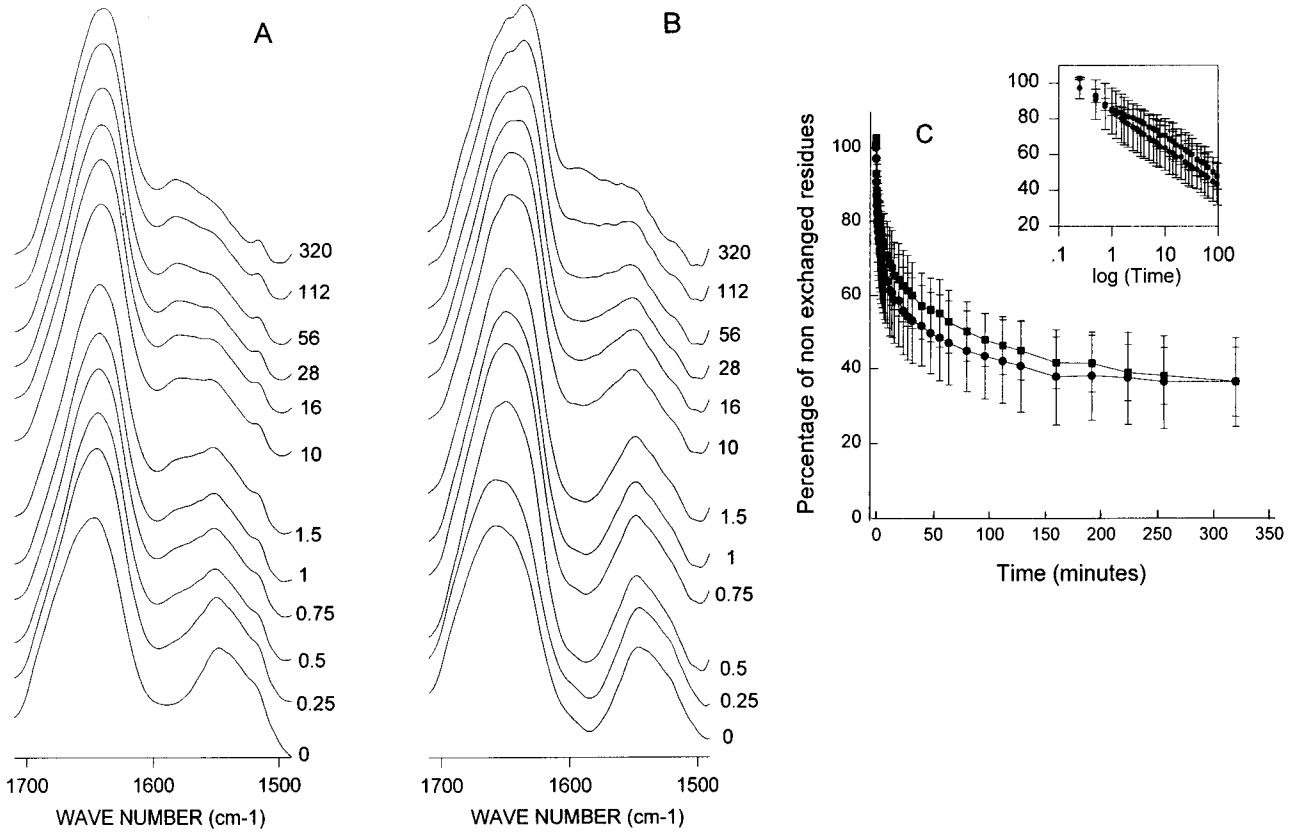

FIGURE 4: Kinetics of H−D exchange in the H132D mutant measured by FTIR. Aerolysin was obtained by treating proaerolysin with trypsin, and the propeptide was removed by gel filtration as described in Experimental Procedures. Spectra of proaerolysin and mature aerolysin mutants were recorded as a function of the exposure time to N_2-saturated D_2O, indicated in minutes in the right margin of the figures. Each group of kinetic spectra corresponds to one of three independent experiments: (A) original H132D proaerolysin spectra, (B) original H132D aerolysin spectra, and (C) evolution of nonexchanged residues in H132D proaerolysin (●) and aerolysin (■) as a function of deuteration time. The percentage of nonexchanged residues was evaluated from the ratio of area amide II:area amide I′ as described in Experimental Procedures. Each curve is the mean of three or four independent experiments, and the error bars represent the standard deviation. The early time points are shown on a log scale as an inset.

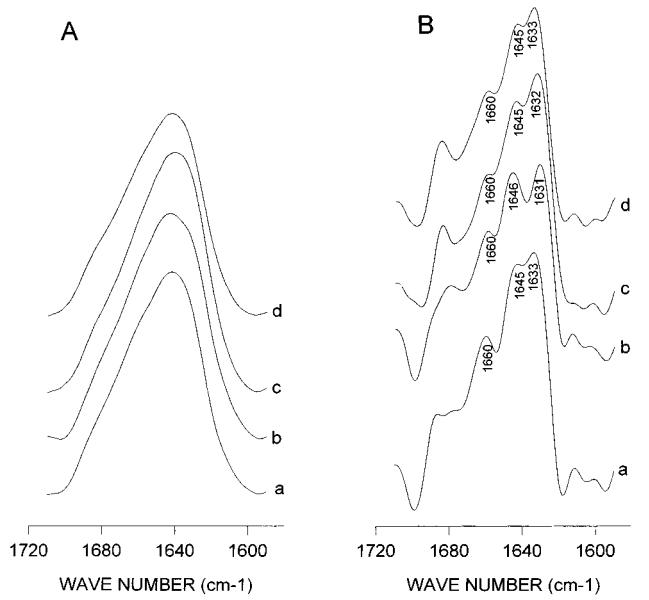

FIGURE 5: Deuterated FTIR spectra of proaerolysin and aerolysin mutants containing engineered disulfide bridges. The aerolysin forms were obtained by treating proaerolysin with trypsin, and the propeptide was removed by gel filtration as described in Experimental Procedures. The spectra of proaerolysin and mature aerolysin mutants were recorded on thin films and taken after the end of the measurements of the corresponding kinetics of deuteration. For all spectra, a linear baseline was subtracted between 1705 and 1595 cm^{-1}: (A) original spectra of M41C proaerolysin (a), M41C aerolysin (b), G202C/I445C proaerolysin (c), and G202C/I445C aerolysin (d); and (B) corresponding deconvoluted spectra with a resolution factor *K* of 2.2.

activation on G202C/I445C proaerolysin, in which the propeptide is covalently linked to the mature protein by a disulfide bridge (*14*). As shown in Figure 5, cleavage of this mutant protein by trypsin did not lead to the conformational change observed with H132D, evidence that the release of the peptide was responsible for the change in secondary structure.

The effect of activation was also studied using a third mutant which is also unable to oligomerize. This is M41C, in which an intermolecular disulfide bridge joins the two Domains 1 in the dimer (ref 15 and M. W. Parker et al., unpublished results). Interestingly, trypsin treatment did not cause the conformational change observed with H132D (Figure 5), although it correctly processed the protein as shown by SDS electrophoresis (Figure 2B) and mass spectrometry.

Structural Effects of Oligomerization. The structure of the heptamer formed by the wild type toxin was studied next. Interestingly, the spectrum of the heptamer (Figure 6A, spectrum b) was very similar to that of the H132D aerolysin dimer (Figure 3A, spectrum b). Since wild type and H132D proaerolysins had very similar spectra (spectra a in Figures 6A and 3A, respectively), this observation suggests that activation led to the same conformational change in the wild type toxin as in the mutant and that oligomerization did not lead to any further change in secondary structure. However, changes in tertiary structure did occur, at least around certain aromatic residues, since a significant change in the near-UV CD spectrum could be observed upon oligomerization (not shown). Changes in tertiary structure or packing were also revealed by the dramatic decrease in the percentage of exchangeable hydrogens in the oligomer as compared to that in proaerolysin (Figure 7). Whereas, within the first 25 min, 55% of the peptide hydrogens exchanged with deuterium

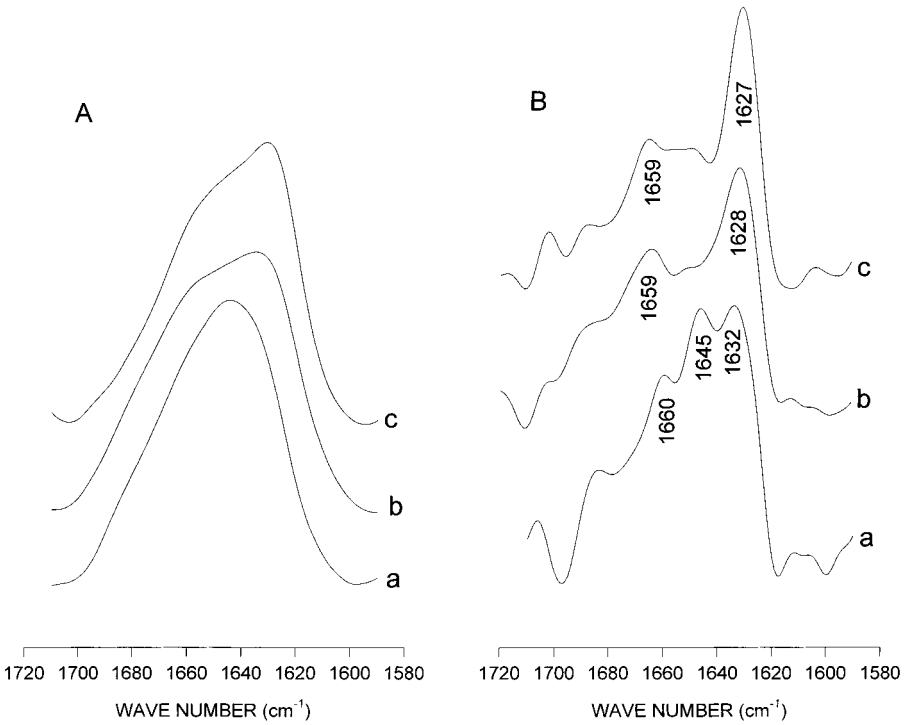

FIGURE 6: Deuterated FTIR spectra of the different forms of the wild type toxin. Aerolysin heptamer (b) was obtained by trypsin cleavage of proaerolysin (a) followed by extensive dialysis as described in Experimental Procedures. As shown in Figure 2A, this sample contained mainly heptameric aerolysin, although a slight contamination by nonoligomerized aerolysin could be detected. Heptameric aerolysin was reconstituted into DMPC vesicles (c) as described in Experimental Procedures. The spectra of proaerolysin (a), heptameric aerolysin (b), and the heptamer reconstituted into DMPC vesicles (c) were recorded on thin films and taken at the end of the measurement of the corresponding kinetics of deuteration. For all spectra, a linear baseline was subtracted between 1705 and 1595 cm^{-1}: (A) original spectra and (B) deconvoluted spectra with a resolution factor *K* of 2.2. The water vapor has been subtracted as described in ref 19.

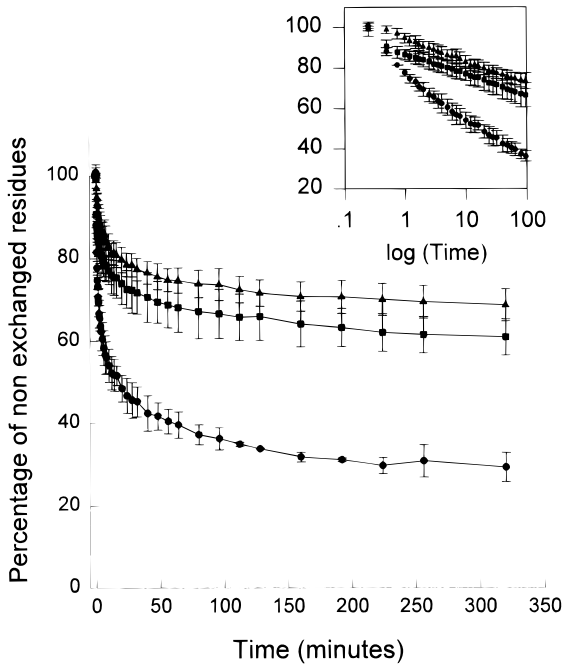

FIGURE 7: Evolution of nonexchanged residues in the wild type toxin as a function of the deuteration time. Heptameric aerolysin in solution and reconstituted into DMPC vesicles were prepared as described for Figure 6. Kinetics of deuteration were measured for proaerolysin, heptameric aerolysin, and the heptamer reconstituted into DMPC vesicles. The percentage of nonexchanged residues was then evaluated from the ratio of area amide II:area amide I′ as described in Experimental Procedures. Each curve is the mean of three or four independent experiments, and the error bars represent the standard deviations: proaerolysin (●), aerolysin (■), and aerolysin reconstituted in DMPC vesicles (▲). The early time points are shown on a log scale as an inset.

upon exposure of proaerolysin to D_2O, less than 30% of the residues were exchanged in the heptamer (Figure 7). This dramatic decrease in H−D exchangeability might be due to the fact that previously exposed regions are involved in monomer−monomer interactions. However, the extreme stability of the aerolysin heptamer probably also contributes to the reduced exchange.

Structural Effects of Membrane Insertion. FTIR analysis of heptameric aerolysin−DMPC vesicles suggested that the lipids induce little modification of the shape of the spectra (Figure 6, spectra c and b, respectively). Only a slight increase in intensity was observed near 1627 cm^{-1}, suggesting an increase in β-sheet structure. Using a curve fitting procedure, a 4% increase of the β-sheet content was estimated with a concomitant decrease in the amount of turn structure. This change is within the experimental error of the method. The presence of lipids did lead to a narrowing of the components at 1659 and 1627 cm^{-1}, suggesting that the hydrogen bonding pattern was more homogeneous after membrane insertion. Some differences could also be observed between the 1659 and 1627 cm^{-1} components as well as in the 1680 cm^{-1} region. However, since the spectra are extremely sensitive to water vapor, even though water vapor components were subtracted from these spectra, we cannot definitively conclude that the observed difference are due to structural modifications.

The percentage of hydrogens exchanged was only slightly lower in the presence of lipids (Figure 7), suggesting that only a small portion of the protein penetrates into the membrane. The difference in hydrogen exchange between

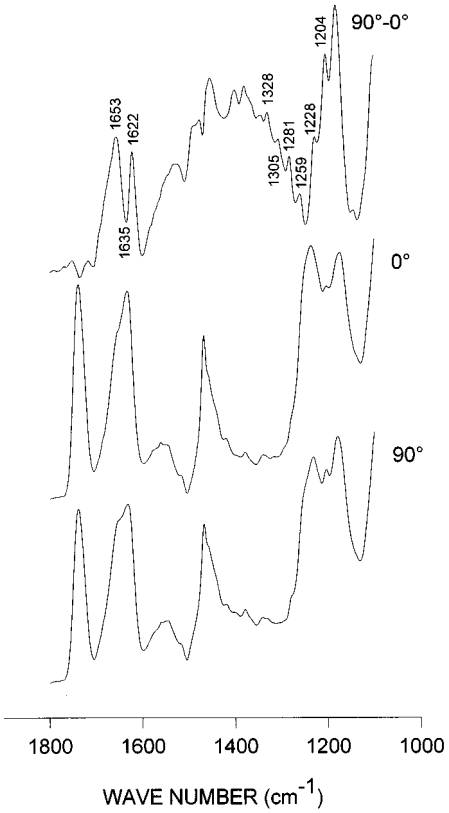

FIGURE 8: Polarized spectra of the aerolysin heptamer reconstituted into DMPC vesicles. The subtraction coefficient for spectrum c was chosen in order to zero the $\nu_{C=O}$ lipid area and was equal to 1.29. The OD scale was 0.12 for the 90° spectrum, 0.078 for the 0° spectrum, and 0.025 for the difference spectrum.

the heptamer in the presence of lipids and proaerolysin is consistent with the difference in calculated solvent accessible surfaces of the two forms of the toxin (≈20% difference based on the model of the channel proposed by M. W. Parker et al. in ref 10) (Table 1).

The orientation of the various secondary structure elements in the heptamer with respect to the membrane was assessed by carrying out measurements with light polarized both horizontally and vertically (Figure 8). The proper orientation of the lipid acyl chains was confirmed by the presence of the peaks in the 1200−1350 cm^{-1} range (peaks at 1204, 1228, 1259, 1281, 1305, and 1328 cm^{-1}). In DMPC, the hydrocarbon chain in the α-position in the gel state is *all-trans* from the ester group to the methyl group, allowing a resonance to occur between the ester group and the CH_2 groups of the chain. This gives rise to the so-called γw-(CH2) progression between 1200 and 1350 cm^{-1} (*16*). The peak at 1204 cm^{-1} was chosen to characterize the lipid acyl chain orientation (*16*). The strong 90° polarization of this absorption peak indicates that the *all-trans* hydrocarbon chain of DMPC was oriented nearly normal to the germanium surface. The dichroic ratio, measured from the absorbance ratio (A_{90}/A_0), was 10−12. Accordingly, the maximum tilt between acyl chain and a normal to the germanium plate was 15−20°. The two positive absorption peaks at 1653 and 1622 cm^{-1}, characteristic of α-helices and β-sheet, respectively, indicate that the C═O bonds were perpendicular to the plane of the membrane. These peaks suggest the presence of a population of α-helices whose axes were perpendicular to the plane of the membrane and a population of β-sheet whose axes were parallel to it. The negative

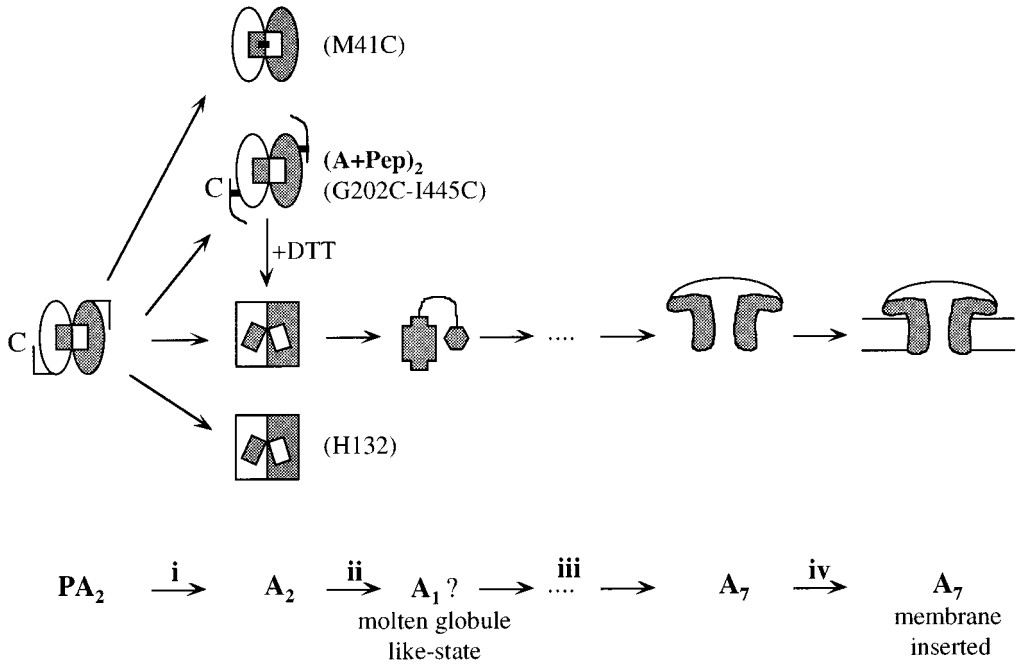

FIGURE 9: Schematic outline of the pathway for aerolysin assembly. On the basis of the present study and previous data in the literature, we propose the following schematic outline for the assembly of the aerolysin heptamer. Proaerolysin (PA) is secreted by the producing bacterium as a dimer (PA2). One monomer is shown in gray and the other in white; the two Domains 1, which are represented as rectangles, clasp each other in a crossover fashion. (i) Activation leads to changes in secondary structure and to a movement of Domains 1 relative to one another. These changes do not occur either if the propeptide is not released (G202C/I445C**,** a mutant which has an engineered disulfide bridge between the propeptide and mature toxin) or if a disulfide bond links the two Domains 1 in the dimer (M41C). The two mutants which are unable to oligomerize, unless the engineered disulfide bonds are reduced, remain inactive dimers. The M41C disulfide bridge can be prevented from forming during the production of the protein by the addition of reducing agents but cannot be broken once it has formed because it is inaccessible. (ii) Circumstantial evidence presented in the text suggests that the dimer separates before heptamer assembly occurs, but the aerolysin monomer has, as yet, never been seen during the oligomerization process. However, the monomer can be obtained by treatment with low amounts of SDS and was shown to adopt a molten globule-like conformation (*2*). Therefore, monomer formation is expected to involve only a change in tertiary structure and not in secondary structure. (iii) Transition to the aerolysin heptamer, which is likely to involve several yet undefined steps, again involves only a change in tertiary structure and not of secondary structure. (iv) Finally, insertion into the lipid membrane also does not involve major secondary structure conformational changes: PA, proaerolysin; and A, aerolysin. The numbers in subscript indicate the oligomeric states of the protein. In parentheses are indicated the mutant toxins which were used to analyze a given state.

deviation observed at 1635 cm^{-1} (0° preferential absorption) suggests the presence of a β-sheet population with an orientation normal to the plane of the membrane, possibly transmembrane. The amount of β-sheet having the latter orientation was estimated to correspond to 13 ± 5% of the protein, corresponding to 55 ± 21 residues.

DISCUSSION

To form a channel, proaerolysin must be proteolytically activated, then oligomerize, and finally insert into the lipid bilayer. Activation of proaerolysin by trypsin results in the removal of 43 amino acids from the C terminus (*8*, *14*). It has not been clear why release of the peptide confers the ability to oligomerize on the toxin, but the present data suggest a possible explanation. Our results show that activation is accompanied by a change in secondary structure characterized by an increase in the amount of β-sheet and a decrease in disordered structure. This conformational change is not due to peptide bond hydrolysis but requires release of the propeptide as we have shown using the G202C/I445C mutant (Figures 5 and 9). More interestingly, the conformational change does not occur in the M41C mutant in which the two Domains 1 are linked by a disulfide bridge, more then 50 Å away from the activation site. This suggests that the conformational change is not restricted to the vicinity of the proteolytic cleavage site but propagates along the molecule, or through monomer−monomer contacts, all the way to Domain 1. As mentioned above, this domain is thought to stabilize the dimer through domain-swapping interactions (ref 10 and M. W. Parker et al., unpublished). Activation may induce a crucial change in the relative positioning of Domains 1 that leads to separation of the monomers (Figure 9). Circumstantial evidence indicates that it is monomers that form the oligomer. There are an odd number of monomers in the oligomer, and they are parallel to each other; they are antiparallel in the dimer (*2*, *10*, *11*, *27*). Since the H132D mutant, which undergoes the same conformational change as the wild type toxin upon activation, is unable to oligomerize, the movement of Domain 1 does not appear to be sufficient to trigger polymerization. Therefore, it seems likely that additional mechanisms such as protonation of His-132 are involved (*26*).

A change in secondary structure upon activation is compatible with the crystal structure of proaerolysin which shows that the propeptide forms extensive contacts with the rest of Domain 4. Loss of the propeptide would lead to large conformational rearrangements in Domain 4 due to the exposure of a buried hydrophobic patch and the loss of contributing strands to the existing β-sheet structure. The increase of β-sheet content of about 10 ± 5% with a concomitant loss in random structure observed by FTIR could be due in part to portions of the long loops at the tip of

Domain 4 taking up some β-structure on loss of the propeptide. As indicated by the present data, other increases are likely to occur throughout the molecule. Since some of the strands in Domain 4 straddle the molecule from tip to tip, it is easy to envisage that conformational changes in Domain 4 upon activation could be propagated throughout the molecule. The observation that no structural changes are observed unless the propeptide is released is also compatible with the crystal structure; the site of proteolytic cleavage is located in a highly flexible, surface-exposed loop, and clipping at this site would have no structural consequences.

The FTIR analysis also led to the unexpected conclusion that secondary structure is unaffected by oligomerization. Only tertiary rearrangements could be observed, and they were not surprising since packing of the monomers in the oligomer is likely to be associated with side chain movements for optimizing interactions. Concomitant with oligomerization, many hydrogens became completely inaccessible to deuterium exchange, either because secondary structure elements became hidden in the monomer−monomer interfaces or because of the extraordinary stability of the heptameric complex (*27*). Similar observations have been made for anthrax toxin protective antigen and *Staphylococcus aureus* α-toxin, which both have functional similarities with respect to aerolysin (*28*). A tertiary conformational change without major secondary structure change was observed upon oligomerization of staphylococcal α-toxin as shown by CD spectroscopy and differential susceptibility to proteases in the different forms (*29*−*31*). More recently, it has been shown that heptamerization of anthrax toxin protective antigen also involves only minor conformational changes, on the basis of the comparison of the crystal structures of the monomer and of the soluble nonlytic heptamer (*32*).

We also analyzed the structure of the aerolysin heptamer in the presence of DMPC. Again, the secondary structure was found to be quite similar to that of the dimer and the heptamer in solution. In contrast, an increase in β-sheet content was found upon membrane insertion of staphylococcal α-toxin (*31*). This difference could be explained by the fact that α-toxin first forms a nonlytic pre-pore which then inserts into the membrane, presumably upon folding of the (initially flexible) insertion peptides into a β-barrel structure (*33*). Currently, there is no evidence for the existence of a nonlytic oligomer of aerolysin, and therefore, there is no reason to believe that the heptamer can adopt different conformations.

As mentioned above, a model of the heptameric form of aerolysin has previously been proposed on the basis of the crystallographic structure of the proaerolysin dimer and electron microscopy (EM) images of the membrane-bound heptamer (*10*, *11*). The EM images showed the heptamer to be mushroom-shaped with the stalk spanning the membrane bilayer. The L-shaped monomer from the crystal structure was fitted into the L-shaped repeating unit of the oligomer, providing a unique fit of the crystal structure to the EM images. The only required alterations to the crystal structure were a rotation of Domain 1 with respect to the large lobe (domains 2−4) and removal of the propeptide. Domains 1 and 2 formed the "flange" of the mushroom-shaped heptamer, while Domains 3 and 4 formed the stalk. Assuming the β-strands in Domain 4 were retained on toxin activation, it was suggested that Domain 4 must form a continual β-sheet with the same domain in the other monomers since only this topology would be energetically favorable in the membrane environment.

Although the heptamer model derived this way is probably correct in gross detail, the fine detail of the model is likely wrong. For example, it was assumed in constructing the heptamer model that there were no structural changes upon removal of the propeptide and the positioning of Domain 1 with respect to the rest of the monomer was rather arbitrary. It was possible to construct the β-barrel stalk of the heptamer with either two or three strands per monomer. The experimental data reported in this paper provide some constraints on the published model and will be useful in fine-tuning or in producing new models of the aerolysin channel.

Studies of the orientation of oligomer secondary structures calculated by dichroic FTIR indicate that most α-helices have their axis oriented perpendicular to the plane of the membrane in contrast to what is predicted by the model. This observation suggests that a more pronounced rotation of Domain 1, which contains about one-third of the helical content of the molecule, relative to the large lobe of the molecule is required. Unfortunately, the errors involved in the FTIR measurements and thereby the error in calculation of β-sheet content perpendicular to the membrane (55 ± 21 residues) do not allow us to distinguish between models where each monomer contributes two or three strands to the transmembrane β-barrel. In the former case, there would be 60 residues in perpendicular strands, whereas in the latter case, there would be 72. However, in the two-stranded model, only 22 residues would span the membrane, and this would be consistent with the H−D exchangeability results where there is little change in exchangeable residues upon membrane insertion.

In the previously reported model of membrane insertion (*10*), it was not clear whether the conformational changes required to convert the water-soluble dimer to the membrane-bound heptamer occurred on activation, dissociation of the dimer, oligomerization, or combinations of the various steps. The data here show that the conformational changes to secondary structure occur very early, at the activation step (Figure 9). Moreover, the changes are not restricted to the vicinity of the cleavage site but propagate all the way to Domain 1. Since Domain 1 has been implicated in dimerization, we speculate that movement of this domain is required for subsequent oligomerization to occur. Oligomerization involves no further change in secondary structure and implies only tertiary rearrangements in the protein. Finally, pore formation appears to involve penetration of only a relatively minor portion of the protein into the lipid bilayer.

ACKNOWLEDGMENT

J. Gruenberg, C. Lesieur, and B. Vecsey-Semjen are gratefully acknowledged for their critical reading of the manuscript.

REFERENCES

1. Parker, M. W., van der Goot, F. G., and Buckley, J. T. (1996) *Mol. Microbiol. 19,* 205−212.
2. van der Goot, F., Ausio, J., Wong, K., Pattus, F., and Buckley, J. (1993) *J. Biol. Chem. 268,* 18272−18279.
3. Howard, S. P., and Buckley, J. T. (1982) *Biochemistry 21,* 1662−1667.

4. Gruber, H. J., Wilmsen, H. U., Cowell, S., Schindler, H., and Buckley, J. T. (1994) *Mol. Microbiol. 14,* 1093−1101.
5. Nelson, K. L., Raja, S. M., and Buckley, J. T. (1997) *J. Biol. Chem. 272,* 12170−12174.
6. Cowell, S., Aschauer, W., Gruber, J. H., Nelson, K. L., and Buckley, J. T. (1997) *Mol. Microbiol.* (in press).
7. Howard, S. P., and Buckley, J. T. (1985) *J. Bacteriol. 163,* 336−340.
8. van der Goot, F. G., Lakey, J. H., Pattus, F., Kay, C. M., Sorokine, O., Van Dorsselaer, A., and Buckley, T. (1992) *Biochemistry 31,* 8566−8570.
9. van der Goot, F. G., Wong, K. R., Pattus, F., and Buckley, J. T. (1993) *Biochemistry 32,* 2636−2642.
10. Parker, M. W., Buckley, J. T., Postma, J. P. M., Tucker, A. D., Leonard, K., Pattus, F., and Tsernoglou, D. (1994) *Nature 367,* 292−295.
11. Wilmsen, H. U., Leonard, K. R., Tichelaar, W., Buckley, J. T., and Pattus, F. (1992) *EMBO J. 11,* 2457−2463.
12. Buckley, J. T. (1990) *Biochem. Cell Biol. 68,* 221−224.
13. Green, M. J., and Buckley, J. T. (1990) *Biochemistry 29,* 2177−2180.
14. van der Goot, F. G., Hardie, K. R., Parker, M. W., and Buckley, J. T. (1994) *J. Biol. Chem. 269,* 30496−30501.
15. Hardie, K. R., Schulze, A., Parker, M. W., and Buckley, J. T. (1995) *Mol. Microbiol. 17,* 1035−1044.
16. Fringeli, U., and Günthard, H. (1981) *Mol. Biol. Biochem. Biophys. 31,* 270−332.
17. Goormaghtigh, E., Cabiaux, V., and Ruysschaert, J. M. (1994) Physical methods in the Study of Biomembranes, in *Subcellular Biochemistry* (Hilderson, H. J. a. R., Ed.) Vol. 23, pp 363−403, Plenum Press, New York.
18. Susi, H., Timaseff, S. N., and Stevens, L. (1967) *J. Biol. Chem. 242,* 5466−5466.
19. Cabiaux, V., Brasseur, R., Wattiez, R., Falmagne, P., Ruysschaert, J. M., and Goormaghtigh, E. (1989) *J. Biol. Chem. 264,* 4928−4938.
20. Goormaghtigh, E., Vigneron, L., Scarborough, G. A., and Ruysschaert, J. M. (1994) *J. Biol. Chem. 269,* 27409−27413.
21. de Jongh, H. H. J., Goormaghtigh, E., and Ruysschaert, J. M. (1995) *Biochemistry 35,* 172−179.
22. Raussens, V., Narayanaswami, V., Goormaghtigh, E., Ryan, R. O., and Ruysschaert, J.-M. (1996) *J. Biol. Chem. 271,* 23089−23095.
23. Laemmli, U. K. (1970) *Nature 227,* 680−685.
24. Kabsch, W., and Sander, C. (1983) *Biopolymers 22,* 2577−2637.
25. Wilmsen, H. U., Buckley, J. T., and Pattus, F. (1991) *Mol. Microbiol. 5,* 2745−2751.
26. Buckley, J. T., Wilmsen, H. U., Lesieur, C., Schultze, A., Pattus, F., Parker, M. W., and van der Goot, F. G. (1995) *Biochemistry 34,* 16450−16455.
27. Moniatte, M., van der Goot, F. G., Buckley, J. T., Pattus, F., and Van Dorsselaer, A. (1996) *FEBS Lett. 384,* 269−272.
28. Lesieur, C., Abrami, L., Fivaz, M., and van der Goot, F. G. (1997) *Mol. Membr. Biol. 14,* 45−64.
29. Tobkes, N., Wallace, B. A., and Bayley, H. (1985) *Biochemistry 24,* 1915−1920.
30. Walker, B., Braha, O., Cheley, S., and Bayley, H. (1995) *Chem. Biol. 2,* 99−105.
31. Vecsey-Semjen, B., Lesieur, C., Möllby, R., and van der Goot, F. G. (1997) *J. Biol. Chem. 272,* 5709−5717.
32. Petosa, C., Collier, R. J., Klimpel, K. R., Leppla, S. H., and Liddington, R. C. (1997) *Nature 385,* 833−838.
33. Song, L., Hobaugh, M. R., Shustak, C., Cheley, S., Bayley, H., and Gouaux, J. E. (1996) *Science 274,* 1859−1866.
34. Kraulis, J. P. (1991) *J. Appl. Crystallogr. 24,* 946−950.

BI971216P